The EMBO Journal Vol.18 No.4 pp.815–821, 1999

Cryo-electron microscopy structure of an SH3 amyloid fibril and model of the molecular packing

José L.Jiménez[1], J.Iñaki Guijarro[2,3], Elena Orlova[4], Jesús Zurdo[2], Christopher M.Dobson[2,5], Margaret Sunde[2,6] and Helen R.Saibil[1,5]

[1]Department of Crystallography, Birkbeck College, Malet Street, London, WC1E 7HX, [2]Oxford Centre for Molecular Sciences, New Chemistry Laboratory, University of Oxford, South Parks Road, Oxford, OX1 3QT and [4]Department of Biochemistry, Imperial College of Science, Technology and Medicine, London, SW7 2AY, UK

[3]Present address: Laboratoire de RMN, Département SIDA-Retrovirus, Institut Pasteur, 28 rue du Dr Roux, 75015 Paris, France
[6]Present address: Department of Biochemistry, University of Cambridge, 80 Tennis Court Road, Cambridge, CB2 1GA, UK

[5]Corresponding authors
e-mail: h.saibil@mail.cryst.bbk.ac.uk

Amyloid fibrils are assemblies of misfolded proteins and are associated with pathological conditions such as Alzheimer's disease and the spongiform encephalopathies. In the amyloid diseases, a diverse group of normally soluble proteins self-assemble to form insoluble fibrils. X-ray fibre diffraction studies have shown that the protofilament cores of fibrils formed from the various proteins all contain a cross-β-scaffold, with β-strands perpendicular and β-sheets parallel to the fibre axis. We have determined the three-dimensional structure of an amyloid fibril, formed by the SH3 domain of phosphatidylinositol-3′-kinase, using cryo-electron microscopy and image processing at 25 Å resolution. The structure is a double helix of two protofilament pairs wound around a hollow core, with a helical crossover repeat of ~600 Å and an axial subunit repeat of ~27 Å. The native SH3 domain is too compact to fit into the fibril density, and must unfold to adopt a longer, thinner shape in the amyloid form. The 20×40-Å protofilaments can only accommodate one pair of flat β-sheets stacked against each other, with very little inter-strand twist. We propose a model for the polypeptide packing as a basis for understanding the structure of amyloid fibrils in general.

Keywords: amyloid fibrils/cryo-electron microscopy/protein misfolding/SH3 domain/single particle analysis

Introduction

There are at least 16 types of human disease associated with the deposition of protein fibrils resulting in tissue damage and degeneration (Pepys, 1996). Amyloid fibrils are formed by polymerization of abnormal states of normally soluble proteins or peptides (Kelly, 1998). These precursor proteins have no general sequence or three-dimensional (3D) structural homology in their native, soluble forms, but they all assemble into a cross-β-fibre structure, with β-strands perpendicular and β-sheets parallel to the fibre axis (Sunde *et al*., 1997). The common core structure of amyloid fibrils has been demonstrated by X-ray fibre diffraction of a wide range of fibril types, based on the presence of a 4.7-Å inter-strand spacing along the fibre axis and a 9–10-Å inter-sheet spacing perpendicular to the axis (Sunde *et al*., 1997). In the case of transthyretin, the native fold is mainly β-sheet, and the unfolding of a small part of the structure may be sufficient to allow its assembly into amyloid (Kelly, 1998). In contrast, the structurally defined part of the cellular prion protein PrP^c is mainly α-helical, and is expected to undergo substantial refolding on conversion to the scrapie (amyloid) form (Riek *et al*., 1996).

Structural studies have been hindered by the disorder and inhomogeneity of amyloid fibril preparations. Negative-stain electron microscopy (EM) studies show long fibrils with diameters of 60–120 Å (Cohen *et al*., 1982), and sometimes long helical pitch repeats of several hundred Ångstroms. X-ray fibre diffraction consistently reveals meridional spacings of 4.7 and 2.4 Å corresponding to the β-strand repeat, as well as more variable equatorial reflections at larger spacings, possibly related to the β-sheet separation and protofilament packing in the fibril assembly. On the basis of fibre diffraction, Blake and Serpell (1996) have proposed a model for the protofilament core of transthyretin amyloid with a 15° twist between adjacent β-strands. So far there has been little information between the very low resolution image features from microscopy and the high resolution meridional diffraction, and an overall 3D picture of fibril structure has been lacking. Therefore, it has not been possible to determine the arrangement of protein subunits and protofilaments in the fibrils.

It has recently been shown that other proteins, in addition to the 16 known to be disease associated, can aggregate into amyloid fibrils. Among these is the SH3 domain of the p85α subunit of bovine phosphatidylinositol-3′-kinase (Guijarro *et al*., 1998; Chiti *et al*., 1999). The native fold of this 84-residue domain contains five β-strands arranged in a β-sandwich (Booker *et al*., 1993). At low pH it partially unfolds and slowly assembles into amyloid fibrils (Guijarro *et al*., 1998). Here we present 3D maps of amyloid fibrils assembled from this SH3 domain, which show four protofilaments wound around a hollow core. The maps suggest that the SH3 topology is altered to generate pairs of flat, untwisted β-sheets, and we propose a model for polypeptide packing in the fibrils.

Results

Variable fibril morphology

We have found that the SH3 amyloid fibrils exhibit a variety of forms that evolve over periods of months,

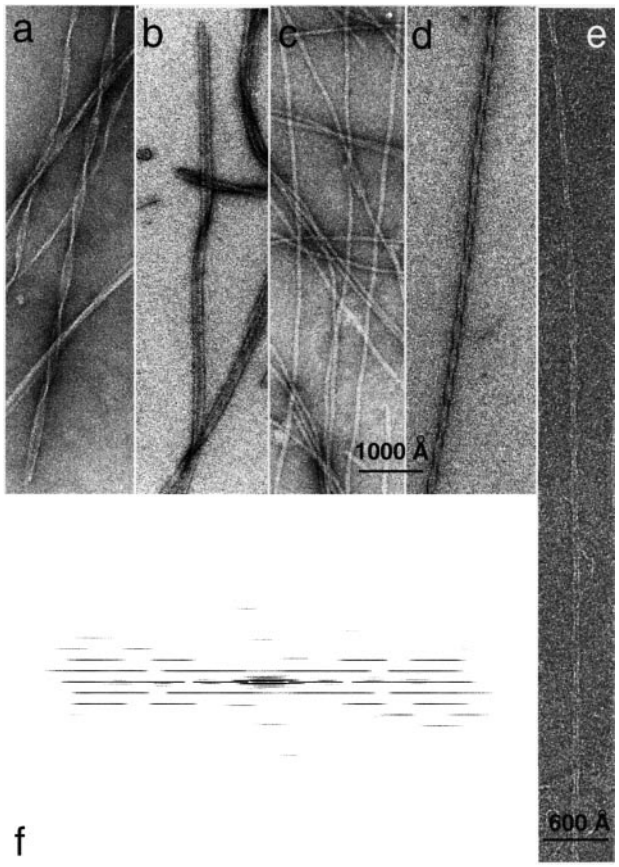

Fig. 1. (**a**–**d**) Negative-stain EM images of SH3 amyloids, showing a range of morphologies similar to those observed with disease-related fibrils (Bauer *et al.*, 1995; Goldsbury *et al.*, 1997; Malinchik *et al.*, 1998). (**e**) Cryo-EM image and (**f**) diffraction pattern of the form seen in (d) with the obvious helical twist, which was used for 3D reconstruction. The layer line spacing is ~600 Å, the repeat unit of the double helix. The various ribbons and smooth fibrils were formed after several months incubation at pH 2.0 (a and b) and pH 2.7 (c) The helical fibres formed at pH 2.0 are seen by negative stain in (d) and cryo-EM in (e). The calculated diffraction pattern (f) was obtained by straightening fibres with PHOELIX software (Carragher *et al.*, 1996), but the axial resolution was limited by variations in the pitch.

closely resembling the range of structures observed for other amyloids formed *in vitro*. The images in Figure 1a–d show a range of twisted and flat ribbons, and smooth and twisted tubular fibres. For structural analysis, we selected a form with a pronounced helical twist, similar to fibrils reported previously for Aβ (1–40), amylin (islet-associated polypeptide) and calcitonin (Bauer *et al.*, 1995; Goldsbury *et al.*, 1997; Malinchik *et al.*, 1998). The diffraction pattern in Figure 1f was calculated from the cryo-EM image in Figure 1e, after interpolation of the fibre to a straight axis. It contains a layer line repeat of ~600 Å, the distance between helical crossovers in the double-helical structure, i.e. the length of the fibril repeat. The precise length of this repeat varied from 545 to 660 Å between different fibres and in different regions of individual fibres. The fibril repeat is one-half the helical repeat, since the structure is a double helix. The evidence for this twofold symmetry is that all layer lines are even (zero phase difference between left and right layer lines in transforms of straightened, individual fibrils).

The diffraction data show structural information to a resolution of 22 Å in the equatorial direction (perpendicular to the fibre axis), but the meridional pattern fades out at ~150 Å due to the variations in the helical pitch. This could be due to angular disorder (variation in angle between successive repeat units along the helix) or stretch (variation in axial spacing between units).

Single particle analysis and classification

To retrieve the structural information lost due to helical disorder, we divided the digitized images of fibrils into individual crossover repeats and treated them as single particles (Boettcher *et al.*, 1996). Eight hundred and ninety cut-out repeats were iteratively aligned and classified by multivariate statistical analysis. This approach enabled us to align the repeats that were naturally straight and sort them into classes according to their length.

The class averages of a 580- and a 610-Å repeat are shown in Figure 2a and e, along with reprojections of 3D maps (see below) calculated from these two repeats (Figure 2b and f), and their diffraction patterns (Figure 2d and h). A subunit repeat is visible in the class average (Figure 2a, expanded view) and sometimes in the raw images (not shown). We determined a subunit periodicity of 27 ± 3 Å from line projections of the class averages (Figure 2c and g).

3D reconstruction

3D maps of the fibrils were calculated from the two best class averages, corresponding to 580- and 610-Å repeats, imposing helical symmetry on the selected repeat units to generate a set of views for filtered back projection. The two independent 3D maps reveal the same features (Figure 3). The surface views and density cross-sections show two pairs of thin protofilaments winding around a hollow core. Regions of weaker density form the extended edges that give the fibrils their characteristic twisting appearance. The protofilaments are ~40 Å apart and ~20 Å thick (Figure 3c and d). The native SH3 domain is a globular structure with a diameter of ~30 Å (Figure 4a and b). It is impossible to fit the fibril density as an assembly of native SH3 domains (yellow surfaces in Figure 4c). If the folded domains are lined up in the protofilaments, these are too thick and the rest of the fibril density is left empty. The domain must unfold to adopt a more extended conformation in order to fit the fibril density.

The ribbon-like protofilaments are shown in a 3D view in Figure 5a. X-ray fibre diffraction of SH3 amyloid shows the 4.7- and 9.4-Å reflections (Guijarro *et al.*, 1998). Although the published fibre-diffraction pattern of SH3 amyloid is not well aligned, these reflections indicate the presence of cross-β-structure as in all the other amyloid fibrils investigated (Sunde *et al.*, 1997). Moreover, Sunde has recently obtained a more aligned diffraction pattern of SH3 fibrils which shows the expected meridional (4.7 Å) and equatorial (9.4 Å) orientations (unpublished data). The 20-Å wide protofilaments can only fit two β-sheets, which must be oriented differently from those in the native fold to make all the strands perpendicular to the fibre axis in the cross-β-structure. The twist between β-strands is also highly restricted by the narrow dimension and long pitch of the protofilaments, implying very flat sheets with an inter-strand angle $<2°$.

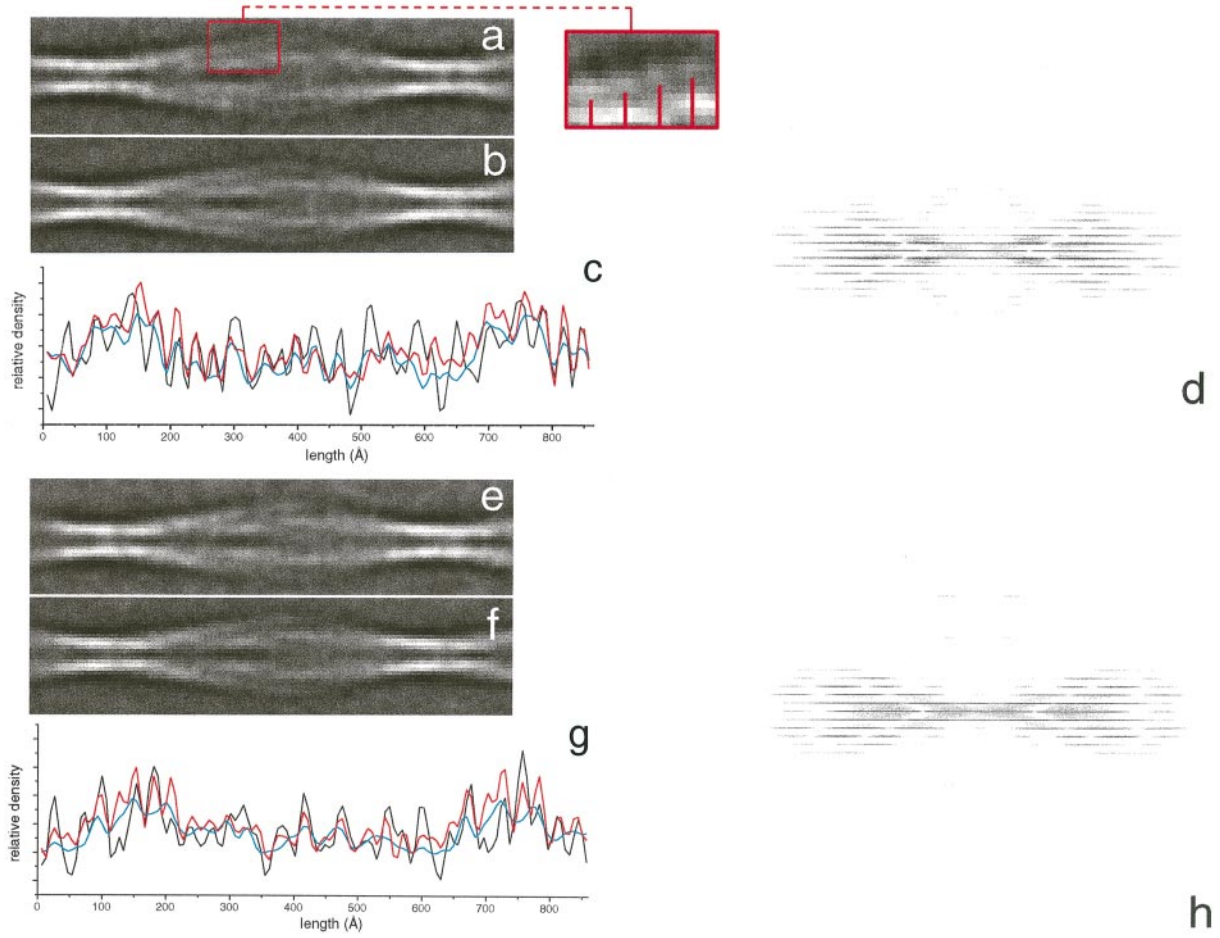

Fig. 2. Class averages (**a** and **e**), reprojections of 3D reconstructions (**b** and **f**), 1D projections (**c** and **g**) and diffraction patterns of the reprojections (**d** and **h**) for the 580- and 610-Å-long repeats, respectively. (In this figure only, the fibre axis is horizontal.) A region in (a) showing a ~30 Å periodicity is enlarged and marked with lines. The good agreement between the input class averages and the reprojections of the 3D maps (compare a with b and e with f), and also between the diffraction pattern of a single fibril (Figure 1f) and of the reprojected maps (g and h), supports the validity of the reconstruction procedure. The line projection comparisons (c and g) show that the 3D maps fit the input images (black line) better when the 27 Å subunit repeat is used in the reconstruction procedure (red) than if the fibre is treated as a continuous helix (blue).

A model for the β-sheet arrangement in the fibrils

In the native fold of the SH3 domain (Figure 4), the two- and three-stranded sheets have their strands at right angles, but fibre-diffraction studies show that the strands must all be 90 ± 5° to the axis of amyloid fibrils (Blake and Serpell, 1996). The axial subunit repeat in the fibrils is ~27 Å, a distance consistent with a five-stranded unit in the cross-β-structure. This suggests a number of simple ways to model the SH3 β-strands into the protofilament structure, assuming that after assembly into the fibril the strands are in regions of the polypeptide chain similar to those in the native structure. For example, each molecule could be incorporated into a single sheet or each molecule could contribute two- or three-stranded sheets to both members of a pair of sheets within a protofilament or to sheets in adjacent protofilaments. These models all generate dimers with two five-stranded β-sheets and the last two are similar to a domain-swapping mechanism (Schlunegger *et al.*, 1997). The fibrils are sometimes seen to split into two thin sub-fibrils. This suggests that individual polypeptide chains could contribute β-strands to each member of a pair of protofilaments. Non-covalent interactions would then provide the bonds assembling the adjacent sub-fibrils into the double-helical structure determined in this work. All three of the suggested strand arrangements are consistent with the observed dimensions of the protofilaments and a five-stranded axial repeat as described above. We do not have any additional evidence from this study which would allow us to discriminate between them or rule out other organizations of the polypeptide chains within the fibrils.

On the basis of the cryo-EM map and the cross-β-structure implied by fibre diffraction, it is possible to construct a model of a rearranged SH3 structure which can be fitted into the EM density of the whole fibril. This is shown in Figure 5 alongside a doubly contoured view of the fibril-density map showing the outer surface as green wire mesh and the higher density protofilaments as blue rendered surfaces. In the model, each protofilament contains a pair of flat β-sheets. The short and long loops connecting the strands are of the right size range to provide the contacts between adjacent protofilaments and to give rise to the diffuse density in the protruding edges of the structure. The visible subunit repeat comes mainly from these edge regions. The surface contour level (mean + 3σ) encloses a volume consistent with the proposed molecular packing.

Any combination of parallel and anti-parallel arrange-

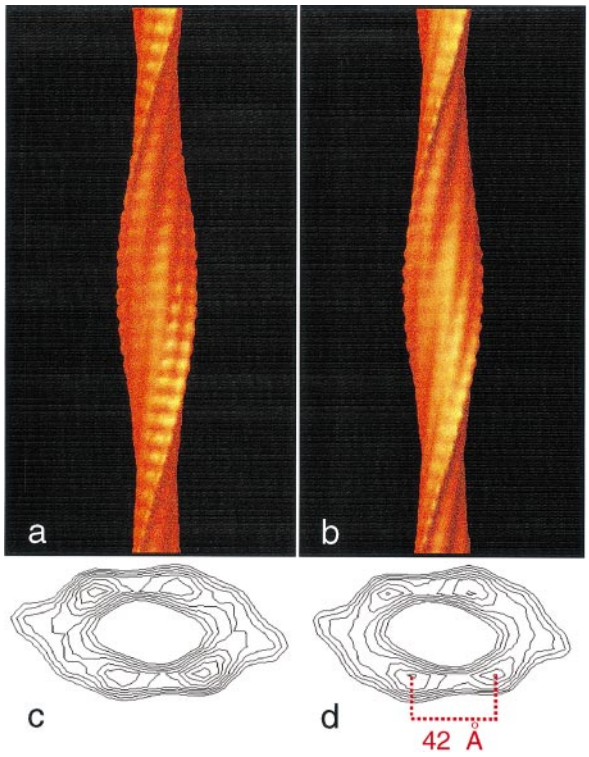

Fig. 3. Three-dimensional reconstructions and contoured density sections of the 610 Å (**a** and **c**) and the 580 Å form (**b** and **d**). The fibrils are shown as rendered surfaces in (a) and (b) (surface is 3σ above the mean density), and as contoured density cross-sections in (c) and (d). The two independent reconstructions are very similar and both show four protofilaments winding around a hollow core, with protruding edge regions. The 27-Å subunit repeat is most pronounced on the edge structures. The subunit repeat was clearly observable in axial 1D projections of the class averages after square root amplitude filtering (Figure 2c and g). The repeat was determined as ~27 Å in both cases, and the exact value used was chosen to give an integral number of subunits in the 580- and 610-Å repeats (21 and 22 subunits respectively). (a) and (b) were produced using AVS (Advanced Visualization System).

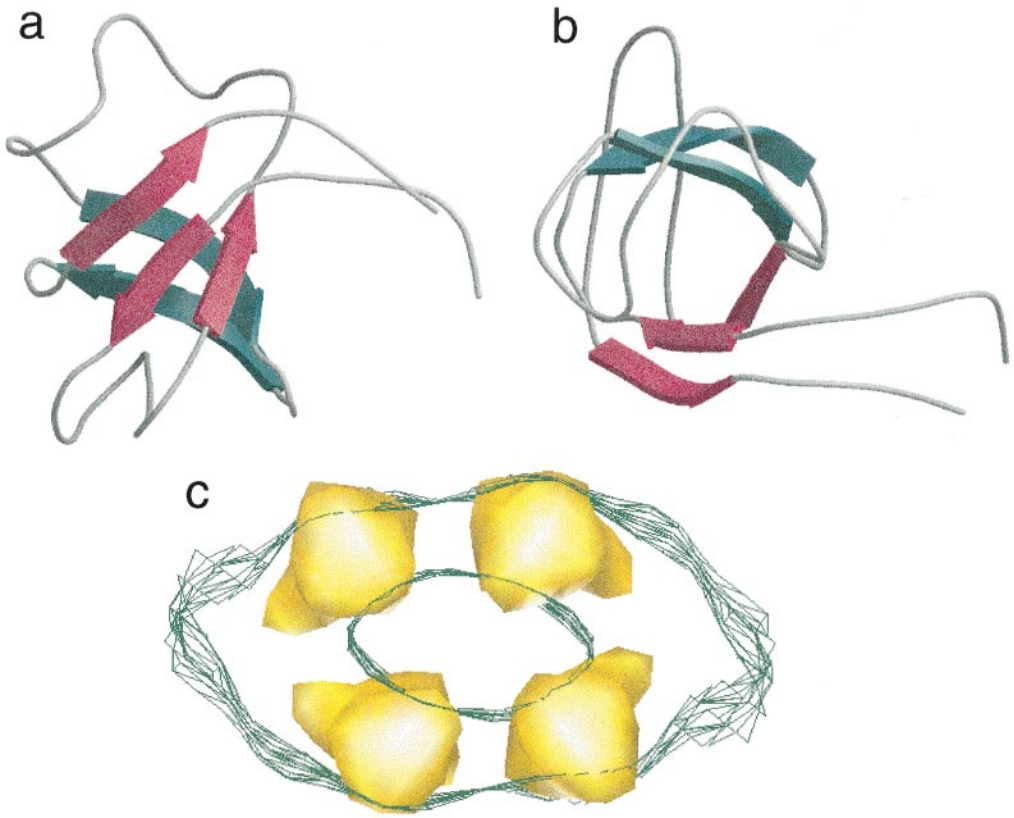

Fig. 4. SH3 domain structure and fit to the fibril density (a and b). Orthogonal views of the SH3 domain structure (Booker *et al*., 1993), showing the native β-sandwich fold. The view in (**b**) was generated by rotating (**a**) towards the viewer by 90°. β-strands in the two orthogonal sheets are coloured magenta and green, and loops are grey. (**c**) The native domain density (yellow), rendered to enclose the molecular volume, was aligned as well as possible into the fibril map (green wire mesh). The native SH3 fold is too rounded to fit the fibril density. In order to fit the map it must unfold to adopt a longer, thinner shape. (a) and (b) were produced using Bobscript (Esnouf, 1997) and Raster3d (Kraulis, 1991; Merritt and Murphy, 1994; Esnouf, 1997); (c) was produced using AVS.

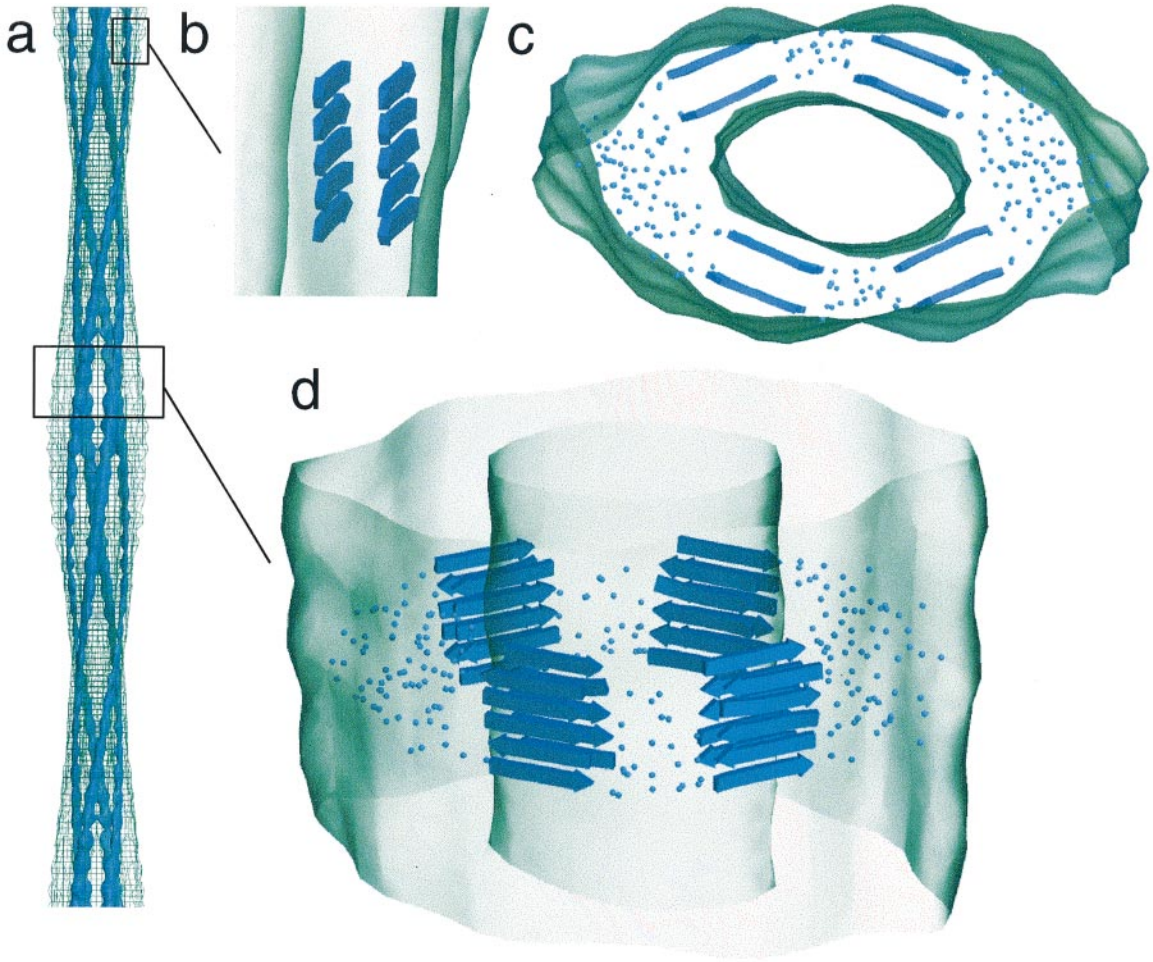

Fig. 5. Modelling the polypeptide fold in the fibril density. (**a**) Overview of the fibril structure, showing the outer surface as green wire mesh and the protofilaments as solid blue surfaces, contoured at a higher density level (4σ above the mean density). The ribbon-like protofilaments form the skeleton of the fibril structure. A model for the molecular packing is shown in (b–d), with the EM map as a transparent rendered surface. (**b**) Side view of a single protofilament, (**c**) cross-section of the fibril and (**d**) slightly tilted side view of the fibril. β-sheets derived from the phosphatidylinositol-3′-kinase SH3 structure have been fitted into the map, after opening the β-sandwich fold and reorienting and straightening the strands. The remaining regions of polypeptide sequence are shown as disconnected dots, to indicate the number of residues present but not the conformation. The β-sheets contain a mixture of parallel and anti-parallel strands. This particular arrangement is arbitrary, and was chosen because it required the least rearrangement of the native β-sheet structure. The β-sheets fit well into the protofilament density, and the loops provide the right amount of mass to generate the rest of the density. The fitting was performed in O (Jones and Kjeldgaard, 1992), and this figure was produced with Bobscript and rendered in Raster 3d (Kraulis, 1991; Merritt and Murphy, 1994; Esnouf, 1997).

ments could equally be accommodated in the structure. The main constraints provided by the observed density are that no more than two sheets can fit into each protofilament, and that strands of ⩽10 residues in length are connected by relatively long loops in the edge regions.

Discussion

The structure of the SH3 amyloid fibril determined here is consistent with that originally proposed for all amyloids by Cooper (1974) and elaborated by Glenner (1980). Key features of the SH3 fibril indicate how different proteins, irrespective of chain length and the native conformation, could be accommodated within a basic amyloid structure. The fibril is composed of a number of protofilaments, four in the case of SH3, which are effectively continuous β-sheets. The edges of the protofilaments can accommodate loops and regions of polypeptide chain which are less tightly packed. These peripheral regions may mediate interactions between the protofilaments. Negative-stain EM, atomic-force microscopy and fibre diffraction of Aβ (1–40) fibrils are consistent with a similar overall morphology, with two sub-fibrils and between three and five protofilaments (Harper *et al*., 1997; Malinchik *et al*., 1998). EM sectioning and fibre-diffraction studies of *ex vivo* transthyretin fibrils suggest that these consist of four protofilaments 50–60 Å in diameter (Serpell *et al*., 1995). The transthyretin protofilament core has been modelled, based on X-ray fibre-diffraction data, as four β-sheets with a 15° twist between adjacent strands (Blake and Serpell, 1996). The two-sheet protofilament model presented here could, however, be extended to a larger number of sheets for the thicker protofilaments. At present there is no evidence to discriminate between twisted and flat β-sheets in the larger protofilament type, but our maps are not consistent with a twisted-sheet configuration for the SH3 protofilaments since they are only 20 Å thick and have a very small overall twist. Although flat, untwisted

β-sheets are unusual in the protein structure database, there are examples, such as part of the β-helix of alkaline protease (Baumann *et al*., 1993), the pectate lyases (Yoder *et al*., 1993) and the p22 tailspike protein (Steinbacher *et al*., 1994).

Pitch variation appears to be a common feature of amyloid fibrils and has hindered structural analysis. The diffraction patterns calculated from the images do not distinguish between twist and stretch disorder as the cause of the variation. However, slight variations in twist between strands in the β-sheet structure could easily account for the pitch variation. Stretch disorder would imply variable spacing between strands, which seems unlikely on the basis of the high-resolution fibre diffraction and the implied hydrogen-bonding network.

The cryo-EM map presented here provides important constraints on how the SH3 polypeptide chain is assembled into amyloid fibrils. Polymerization into fibrils requires at least partial unfolding of native proteins (Booth *et al*., 1997; Kelly, 1998) and is not restricted to proteins whose native fold contains β-sheets. Indeed, formation of fibrils from native states of proteins is frequently associated with a conversion from helical to sheet structure (Horwich and Weissman, 1997; Sunde and Blake, 1997). Even in the case of the SH3 domain studied here, where the native fold is largely β-structure, the structure of the fibrils requires that this must be substantially rearranged relative to that of the native protein. Although amyloid fibrils are associated with disease *in vivo*, it is evident that closely similar fibrils can be formed *in vitro*, even by a protein domain such as SH3 for which no disease state is implicated. This suggests that this type of self-association is a general property of polypeptide chains, albeit one that natural proteins do not readily exhibit under normal physiological conditions (Sunde and Blake, 1997; Chiti *et al*., 1999). The structure reported here provides a first glimpse of this alternative to the familiar globular structures of protein molecules.

Materials and methods

Sample preparation, electron microscopy and helical diffraction

SH3 domains, expressed and purified as described previously (Guijarro *et al*., 1998), were incubated at 10 mg/ml for periods of up to 6 months at pH 2.0 or 2.7. The resulting fibres were vitrified on holey carbon grids, and low-electron-dose images were recorded at 120 kV and 1.3–1.5 μm under-focus on a JEOL 1200 EX microscope with an Oxford Instruments cryotransfer stage at 30 000×. Films were digitized on a Leafscan 45 linear CCD scanner (Ilford Ltd, Cheshire, UK) at a spacing of 10 μm and interpolated to 6.7 Å/pixel for processing.

To calculate helical diffraction patterns, the fibres were straightened using PHOELIX software, by fitting the helical axis to a cubic spline curve and then interpolating the fibre onto a straight line (Carragher *et al*., 1996). Most of the fibres did not diffract beyond one or two layer lines. A similar problem encountered in earlier work with paired helical filaments, another fibrillar structure with variable pitch and low-resolution meridional diffraction, was solved by interpolating the fibre images to a constant pitch (Crowther and Wischik, 1985), followed by helical reconstruction (DeRosier and Moore, 1970).

Single particle analysis

Single particle analysis (Frank, 1996) was performed using either Imagic (van Heel *et al*., 1996) or Spider (Frank *et al*., 1996) software. Digitized fibre images were cut into individual repeats, with overlapping ends to allow for subsequent alignment. The isolated repeats were treated as single particles with the aim of identifying subclasses of straight repeats with the same length. Eight hundred and ninety cut-out repeat units were aligned and then classified by multivariate statistical analysis, using the average of repeats from the straightest fibre as a starting template. Good quality classes had low inter-image variance and gave class averages that were clearly straight and showed polarity, with a high signal-to-noise ratio. This procedure was iterated several times and resulted in two good classes of different length which were used for reconstruction. The shorter repeat contained 92 images and the longer repeat 77. Together, they represent ~19% of the whole data set. The length of the repeat unit in the chosen class averages was determined by cross-correlation of the crossover regions with the whole image. The distances between crossovers were found to be ~580 and ~610 Å.

An approximate axial subunit repeat of 27 ± 3 Å was determined from the one-dimensional (1D) projections of these averages after square-root-amplitude filtering. The values were chosen to give an integral number of subunits per pitch repeat. For the two class averages used, this gives the selection rules $l = n + 42m$ or $l = n + 44m$, respectively, where n and m are integers and n is even. Note that both the helical and subunit repeats are not precisely determined, so that other, similar selection rules are equally possible.

3D reconstruction

Our procedure uses ideas from several earlier approaches to helical disorder correction based on cross-correlation and back projection (e.g. Bluemke *et al*., 1988; Sosa and Milligan, 1996). Because of the helical symmetry, a single view of the repeat unit contains a set of views of the subunit in different orientations, suitable for 3D reconstruction. In this case the structure is a double helix, so the fibril repeat unit covers 180° of rotation. Three-dimensional maps were calculated from the two best class averages by filtered back projection, assuming either a continuous helix or the 27-Å subunit repeat. The overall features of protofilament packing and density cross-section were unaffected by imposition of a subunit repeat, but the line projections (Figure 2c and g) and diffraction patterns (Figure 2d and h) of the reprojected images gave a better match to the input data when the 27 Å repeat was imposed. The diffraction pattern of the reprojected helix gave excellent agreement with the original from the straightened fibre, and showed strong intensity to 22 Å resolution in the equatorial (radial) direction (Figure 1f). Resolution tests by Fourier shell correlation and phase residual between cross-sections of the two maps (Figure 3c and d) show agreement to 25 Å, but there is reliable information to 22 Å in the equatorial direction for each map. The absolute hand is not determined by the method used here and is arbitrary.

Acknowledgements

We thank Bridget Carragher, Ed Morris, Hind AL-Khayat, John Kenney, Steve Fuller, David DeRosier, Erhard Hohenester, Janet Thornton and Iain Campbell for helpful discussions, Richard Westlake, Dave Houldershaw, Claire Naylor and Helen White for help with computing and Juliet Munn and Shaoxia Chen for EM support. We are grateful for support from the Wellcome Trust (J.L.J., C.M.D. and H.R.S.), MRC and EPA Cephalosporin Junior Research Fellowship from Lady Margaret Hall, Oxford (M.S.) BBSRC, MRC and EPSRC (the Oxford Centre for Molecular Sciences), EC (J.I.G. and J.Z.) and an International Research Scholar award from the Howard Hughes Medical Institute (C.M.D.).

References

Bauer,H.H., Aebi,U., Haner,M., Hermann,R., Muller,M., Arvinte,T. and Merkle,H.P. (1995) Architecture and polymorphism of fibrillar supramolecular assemblies produced by *in vitro* aggregation of human calcitonin. *J. Struct. Biol*., **115**, 1–15.

Baumann,U., Wu,S., Flaherty,K.M. and McKay,D.B. (1993) The crystal structure of alkaline protease. *EMBO J*., **12**, 3357–3364.

Blake,C. and Serpell,L.C. (1996) Synchrotron X-ray studies suggest that the core of the transthyretin amyloid fibril is a continuous β-sheet helix. *Structure*, **4**, 989–998.

Bluemke,D.A., Carragher,B. and Josephs,R. (1988) The reconstruction of helical particles with variable pitch. *Ultramicroscopy*, **26**, 255–270.

Boettcher,C., Stark,H. and van Heel,M. (1996) Stacked bilayer helices: a new structural organization of amphiphilic molecules. *Ultramicroscopy*, **62**, 133–139.

Booker,G.W., Gout,I., Downing,A.K., Driscoll,P.C., Boyd,J., Waterfield,M.D. and Campbell,I.D. (1993) Solution structure and

ligand binding site of the SH3 domain of the p85α subunit of phosphatidylinositol 3-kinase. *Cell*, **73**, 813–822.
Booth,D.R. *et al.* (1997) Instability, unfolding and aggregation of human lysozyme variants underlying amyloid fibrillogenesis. *Nature*, **385**, 787–793.
Carragher,B., Whittaker,M. and Milligan,R.A. (1996) Helical processing using PHOELIX. *J. Struct. Biol.*, **116**, 107–112.
Chiti,F., Webster,P., Taddei,A., Clark,A., Stefani,G., Ramponi,G. and Dobson,C.M. (1999) Designing conditions for *in vitro* formation of amyloid protofilaments and fibrils. *Proc. Natl Acad. Sci. USA*, in press.
Cohen,A.S., Shirahama,T. and Skinner,M. (1982) Electron microscopy of amyloid. In Harris,J.R. (ed.), *Electron Microscopy of Proteins*, Vol. 3. Academic Press, London, UK, pp. 165–205.
Cooper,J.H. (1974) Selective staining as a function of amyloid composition and structure: histochemical analysis of the alkaline Congo red, standardized toluidine blue and iodine methods. *Lab. Invest.*, **31**, 232–238.
Crowther,R.A. and Wischik,C. (1985) Image reconstruction of the Alzheimer paired helical filament. *EMBO J.*, **4**, 3661–3665.
DeRosier,D.J. and Moore,P.B. (1970) Reconstruction of the three-dimensional image from electron micrographs of structures with helical symmetry. *J. Mol. Biol.*, **52**, 355–369.
Esnouf,R.M. (1997) An extensively modified version of Molscript that includes greatly enhanced coloring capabilities. *J. Mol. Graphics*, **15**, 132–134.
Frank,J. (1996) *Three-Dimensional Electron Microscopy of Macromolecular Assemblies*. Academic Press, San Diego, CA.
Frank,J., Radermacher,M., Penczek,P., Zhu,J., Li,Y., Ladjadj,M. and Leith,A. (1996) SPIDER and WEB: processing and visualization of images in 3D electron microscopy and related fields. *J. Struct. Biol.*, **116**, 190–199.
Glenner,G.G. (1980) Amyloid deposits and amyloidosis. The β-fibrilloses (part one). *N. Engl. J. Med.*, **302**, 1283–1292.
Goldsbury,C.S. *et al.* (1997) Polymorphic fibrillar assembly of human amylin. *J. Struct. Biol.*, **119**, 17–27.
Guijarro,J.I., Sunde,M., Jones,J.A., Campbell,I.D. and Dobson,C.M. (1998) Amyloid fibril formation by an SH3 domain. *Proc. Natl Acad. Sci. USA*, **95**, 4224–4228.
Harper,J.D., Lieber,C.M. and Lansbury,P.T. (1997) Atomic force microscopic imaging of seeded fibril formation and fibril branching by the Alzheimer's disease amyloid-β protein. *Chem. Biol.*, **4**, 951–959.
Horwich,A.L. and Weissman,J.S. (1997) Deadly conformations—protein misfolding in prion disease. *Cell*, **89**, 499–510.
Jones,T.A. and Kjeldgaard,M. (1992) *O version 5.8.1*. Department of Molecular Biology, University of Uppsala, Sweden.
Kelly,J.W. (1998) The alternative conformations of amyloidogenic proteins and their multi-step assembly pathways. *Curr. Opin. Struct. Biol.*, **8**, 101–106.
Kraulis,P.J. (1991) Molscript—a program to produce both detailed and schematic plots of protein structures. *J. Appl. Crystallogr.*, **24**, 946–950.
Malinchik,S.B., Inouye,H., Szumowski,K.E. and Kirschner,D.A. (1998) Structural analysis of Alzheimer's β (1–40) amyloid: protofilament assembly of tubular fibrils. *Biophys J.*, **74**, 537–545.
Merritt,E.A. and Murphy,M.E.P. (1994) Raster3d version-2.0—a program for photorealistic molecular graphics. *Acta Crystallogr. D*, **50**, 869–873.
Pepys,M.B. (1996) Amyloidosis. In Weatherall,D.J., Ledingham,J.G.G. and Warell,D.A. (eds), *The Oxford Textbook of Medicine*, 3rd edn, Vol. 2. Oxford University Press, Oxford, UK, pp. 1512–1524.
Riek,R., Hornemann,S., Wider,G., Billeter,M., Glockshuber,R. and Wüthrich,K. (1996) NMR structure of the mouse prion protein domain PrP (121–231). *Nature*, **382**, 180–182.
Schlunegger,M.P., Bennett,M.J. and Eisenberg,D. (1997) Oligomer formation by 3D domain swapping: a model for protein assembly and misassembly. *Adv. Protein Chem.*, **50**, 61–122.
Serpell,L.C., Sunde,M., Fraser,P.E., Luther,P.K., Morris,E.P., Sangren,O., Lundgren,E. and Blake,C.C.F. (1995) Examination of the structure of the transthyretin amyloid fibril by image reconstruction from electron micrographs. *J. Mol. Biol.*, **254**, 113–118.
Sosa,H. and Milligan,R.A. (1996) 3-dimensional structure of ncd-decorated microtubules obtained by a back-projection method. *J. Mol. Biol.*, **260**, 743–755.
Steinbacher,S., Seckler,R., Miller,S., Steipe,B., Huber,R. and Reinemer,P. (1994) Crystal structure of p22 tailspike protein—interdigitated subunits in a thermostable trimer. *Science*, **265**, 383–386.
Sunde,M. and Blake,C. (1997) The structure of amyloid fibrils by electron microscopy and X-ray diffraction. *Adv. Protein Chem.*, **50**, 123–159.
Sunde,M., Serpell,L.C., Bartlam,M., Fraser,P.E., Pepys,M.B. and Blake,C.C.F. (1997) The common core structure of amyloid fibrils by synchrotron X-ray diffraction. *J. Mol. Biol.*, **273**, 729–739.
van Heel,M., Harauz,G., Orlova,E., Schmidt,R. and Schatz,M. (1996) A new generation of the IMAGIC image processing system. *J. Struct. Biol.*, **116**, 17–24.
Yoder,M.D., Keen,N.T. and Jurnak,F. (1993) New domain motif—the structure of pectate lyase-c, a secreted plant virulence factor. *Science*, **260**, 1503–1507.

Received October 20, 1998; revised and accepted December 18, 1998